



# CHORUS

This is the accepted manuscript made available via CHORUS. The article has been published as:

## Shubnikov-de Haas oscillations in the bulk Rashba semiconductor BiTeI

C. Bell, M. S. Bahramy, H. Murakawa, J. G. Checkelsky, R. Arita, Y. Kaneko, Y. Onose, M. Tokunaga, Y. Kohama, N. Nagaosa, Y. Tokura, and H. Y. Hwang

Phys. Rev. B **87**, 081109 — Published 28 February 2013

DOI: [10.1103/PhysRevB.87.081109](https://doi.org/10.1103/PhysRevB.87.081109)

# Shubnikov-de Haas oscillations in the bulk Rashba semiconductor BiTeI

C. Bell,<sup>1</sup> M. S. Bahramy,<sup>2</sup> H. Murakawa,<sup>2</sup> J. G. Checkelsky,<sup>2</sup> R. Arita,<sup>2,3</sup> Y. Kaneko,<sup>4</sup> Y. Onose,<sup>3,4</sup> M. Tokunaga,<sup>5</sup> Y. Kohama,<sup>5</sup> N. Nagaosa,<sup>2,3</sup> Y. Tokura,<sup>2,3,4</sup> and H. Y. Hwang<sup>1,2,6</sup>

<sup>1</sup>*Stanford Institute for Materials and Energy Sciences,*

*SLAC National Accelerator Laboratory,*

*Menlo Park, California 94025, USA*

<sup>2</sup>*Correlated Electron Research Group (CERG),*

*RIKEN-ASI, Wako 351-0918, Japan*

<sup>3</sup>*Department of Applied Physics, University of Tokyo, Tokyo 113-8656, Japan*

<sup>4</sup>*Multiferroics Project, ERATO, JST, Tokyo 113-8656, Japan*

<sup>5</sup>*International MegaGauss Science Laboratory, Institute for Solid State Physics,*

*The University of Tokyo, Kashiwa 277-8581, Japan*

<sup>6</sup>*Geballe Laboratory for Advanced Materials, Department of Applied Physics,*

*Stanford University, Stanford, California 94305, USA*

## Abstract

Bulk magnetoresistance quantum oscillations are observed in high quality single crystal samples of BiTeI. This compound shows an extremely large internal spin-orbit coupling, associated with the polarity of the alternating Bi, Te, and I layers perpendicular to the  $c$ -axis. The corresponding areas of the inner and outer Fermi surfaces around the A-point show good agreement with theoretical calculations, demonstrating that the intrinsic bulk Rashba-type splitting is nearly 360 meV, comparable to the largest spin-orbit coupling generated in heterostructures and at surfaces.

The presence of spin-orbit coupling has profound consequences on a material's band structure, and the resulting electronic properties. Although recognized for many years,[1] recently a vast array of fascinating physics and functionalities have emerged, including unconventional superconductivity,[2] the spin Hall effect,[3] and novel topological groundstates.[4, 5] Spin-orbit coupling is also established as a potential route to alternative device architectures.[6] Experimental and theoretical research has been driven by the wide variety of materials in which such appealing physics can be found. Notable examples are traditional semiconductor heterostructures,[7] the Si surface,[8] single crystal metals,[9] and samples with a surface alloy.[10] Thin film metal systems have also provoked recent interest, since the Rashba spin-orbit coupling due to the presence of broken inversion symmetry, can be relatively large.[11] In addition to artificially generated Rashba spin-orbit coupling, (RSOC), essentially identical properties can also be found intrinsically in some materials.

An intriguing example is BiTeI, which possesses large electric polarity along its crystallographic  $c$ -axis. BiTeI belongs to the rhombohedral space group  $P3m1$ , with lattice constants  $a = 4.336 \text{ \AA}$  and  $c = 6.84 \text{ \AA}$ . [12] The crystal structure is schematically shown in Fig. 1(a). Each Bi atom is six-fold co-ordinated by three Te and three I atoms, forming a distorted octahedron. The system can be visualized as layers consisting of Bi, Te and I. Due to the covalency and ionicity of the Bi-Te and Bi-I layers, respectively,[13] the system possesses large internal electric fields between the layers, giving rise to intrinsic RSOC, which is comparable to the largest RSOC found in other systems.[14] Angle-resolved photoemission spectroscopy measurements in these crystals have revealed band structures consistent with the theoretical expectations, assuming a large surface accumulation layer,[14] as has been observed in several related systems.[15–17] Notably a large RSOC has been found at the surface accumulation layer of Bi<sub>2</sub>Se<sub>3</sub>, [17] although by symmetry no bulk Rashba effect is expected.

In this context, it is vital to experimentally probe the bulk band structure of BiTeI. In this Letter, enabled by continuing efforts to refine crystal growth, we present transport measurements of Shubnikov-de Haas (SdH) resistance oscillations in delaminated samples of BiTeI. The temperature and angular dependences of the SdH data show good agreement with the theoretical expectations, for both pieces of the predicted Fermi surfaces.

BiTeI is a degenerate semiconductor, with doping due to non-stoichiometry, much as in Bi<sub>2</sub>Se<sub>3</sub>. Two samples were investigated in this work with slightly different carrier densities.

Magneto-transport measurements were made down to a temperature  $T \sim 2$  K, with applied magnetic fields  $H$  up to  $\mu_0 H = \pm 14$  T, ( $\mu_0$  is the vacuum permeability) for sample #1, and  $\mu_0 H = \pm 57$  T for sample #2. The samples were mounted on a horizontal rotator, with relative angular accuracy of the inclination angle,  $\theta$ , better than  $0.1^\circ$ . However the absolute accuracy, combining the uncertainties of corrugations on the sample and misalignments, was conservatively set as  $\pm 5^\circ$ .

The amplitude of the SdH oscillations in these crystals was relatively small, and combined with the low resistivity, a relatively large current density was needed to achieve a sufficient signal/noise ratio. In order to ameliorate this problem, the absolute resistance was enhanced by delaminating a crystal perpendicular to the  $c$ -axis using double-sided adhesive tape. Electrical contacts were additionally improved with sputter deposited Au at the edges of the crystal.

Density functional theory (DFT) calculations were performed to calculate the band structure of the BiTeI,[20] assuming that doping simply induces a rigid band shift. For sample #1 (#2) the chemical potential corresponding to the bulk electron density  $n = 4.5 \times 10^{19}$   $\text{cm}^{-3}$  ( $4.2 \times 10^{19}$   $\text{cm}^{-3}$ ) is calculated to be 0.151 eV (0.145 eV) above the conduction band minimum. The cyclotron effective mass  $m^*$  was calculated using the relation  $m^* = \frac{\hbar^2}{2\pi} \frac{\partial A_k}{\partial E} \Big|_{E=E_F}$ , [18] where  $A_k$  is the cross sectional area of the Fermi surface (FS) normal to the applied magnetic field,  $\hbar$  the reduced Plank constant, and  $E_F$  the Fermi energy.

According to earlier DFT conclusions,[19] BiTeI has a minimum band gap around the hexagonal face center of its Brillouin zone, referred to as the A-point [see Fig. 1(b)]. For the level of doping measured in relatively thicker crystals, the resulting calculated band splitting in the vicinity of the A-point due to the RSOc and the corresponding Fermi surfaces (FS) are shown in Figs. 1(c) and 2 respectively for the parameters of sample #1. Here, the Rashba energy splitting  $\Delta E_R$  is nearly 360 meV, with a momentum offset  $\Delta k_R \sim 0.05 \text{ \AA}^{-1}$ .  $E_F$  lies just above the Dirac point created by the Rashba split conduction bands at the A-point, such that the FS for this system consists of two distinct parts. Both FS's possess strong two-dimensional character, reflecting the layered nature of the BiTeI crystal. The larger FS, which we refer to as the Outer FS (OFS), is approximately cylindrical, with slight three-fold symmetric corrugations in the  $k_x - k_y$  plane, due to the trigonal symmetry in the plane perpendicular to the  $c$ -axis. The smaller, Inner FS (IFS) is essentially circular in the  $k_x - k_y$  cross-section, and cigar shaped along  $k_z$ , as illustrated in Fig. 2.

Multiple samples exhibited the same behavior; here we focus on transport measurements on two delaminated crystals, using a standard low frequency a.c. resistance bridge, in a van der Pauw geometry, and a bias current in the range 2-10 mA. Focusing first on sample #1, the bulk resistivity in pieces from the same ampoule was measured to be  $1.80 \times 10^{-4} \Omega\text{cm}$ . Using the measured sheet resistance of sample #1, we calculate a thickness in the  $c$ -direction of  $\sim 4.6 \mu\text{m}$ . The Hall resistance showed a slight non-linearity, and a two-carrier fit resulted in densities of  $(4.77 \pm 0.04) \times 10^{19}$  and  $(1.1 \pm 0.2) \times 10^{17} \text{ cm}^{-3}$  for the OFS and IFS carrier densities, respectively, assuming the above thickness, with corresponding Hall mobilities of  $716 \pm 2$  and  $6850 \pm 1000 \text{ cm}^2\text{V}^{-1}\text{s}^{-1}$ . [20]

Quantum oscillations from the IFS showed only a few clear oscillations in the field range as shown in magnetic field dependence of the longitudinal resistivity  $\rho(H)$  in Fig. 3. Since the SdH frequency  $F = F_{\text{IFS}}$  is relatively small, and several full oscillations are not observed, the Fast Fourier Transform (FFT) spectra do not show clear peaks, thus we instead extract  $F_{\text{IFS}}$  directly from the  $\rho(H)$  data, after a linear background has been removed. The arrows in the inset of Fig. 3 show the local maximum and minimum in the data used to define  $F_{\text{IFS}}$ . We use the Onsager relation to relate the SdH frequency  $F$  to the FS area  $A_k$  via  $F = (\Phi_0/2\pi^2)A_k$ , where  $\Phi_0$  is the flux quantum, assuming spin degeneracy is broken by the Rashba splitting as shown in Fig. 1(c). The corresponding  $A_k^{\text{IFS}}(\theta)$  are summarized in Fig. 4, together with the calculated dependence. We obtain excellent agreement between the theoretical and experimentally determined values of  $A_k^{\text{IFS}}$  over a wide range of  $\theta$  for the IFS. Similar data were also measured for sample #2, also summarized in Fig. 4, again showing agreement between the theoretical FS area and the measured  $A_k^{\text{IFS}}(\theta)$ .

Next we turn to the higher frequency SdH oscillations, found at higher fields. These are not observed in Fig. 3 due to their relatively small amplitude. Figure 5(a) shows the temperature dependence of the SdH oscillations for sample #1 at  $\theta = 0^\circ$ , after removing a quartic polynomial background from the magnetoresistance background. [20] Similar high field oscillations could be also found for increasing  $\theta$ , as shown in Fig. 5(b), but with rapidly decreasing amplitude, reaching the noise floor of our measurement at  $\theta \sim 30^\circ$ . The FFT spectrum of the data at  $\theta = 0^\circ$  has a clear peak at  $356.5 \pm 0.6 \text{ T}$ . [20] The above frequency corresponds to a FS area of  $A_k^{\text{OFS}} = 0.03984 \pm 0.00006 \text{ \AA}^{-2}$ , in reasonable agreement with the calculated value of  $0.03472 \text{ \AA}^{-2}$  for the OFS. For  $0^\circ \leq \theta \leq 30^\circ$  we find a small but significant increase of  $F_{\text{OFS}}$  and hence  $A_k^{\text{OFS}}$  with increasing  $\theta$ .

In addition to the temperature dependence of the SdH amplitude at  $\theta = 0^\circ$ , sufficient signal to noise was available to measure a series of different  $T$  also for  $\theta = 15^\circ$ . We fitted these two data sets using the Lifshitz-Kosevich (LF) formula,

$$\frac{\Delta\rho}{4\rho_0} = \exp(-2\pi^2 k_B T_D / \hbar\omega_c) \frac{2\pi^2 k_B T / \hbar\omega_c}{\sinh(2\pi^2 k_B T / \hbar\omega_c)} \quad (1)$$

where  $\rho_0$  is the non-oscillatory component of the resistivity at  $H = 0$  T,  $T_D$  is the Dingle temperature,  $k_B$  Boltzmann's constant and the cyclotron frequency  $\omega_c = e\mu_0 H / m^*$ , where  $e$  is the elementary charge. Using this fit, we first obtain the effective masses of  $0.167 \pm 0.003$  and  $0.161 \pm 0.005$ , in units of the bare electron mass  $m_0$  for  $\theta = 0^\circ$  and  $15^\circ$  respectively. Here the best fit values were calculated by minimizing the sum  $\Sigma = \sum_{\text{data}} (\text{data} - \text{fit})^2$  for various  $m^*$ . The error bars correspond to an increase of  $\Sigma$  by a factor of 5 above the optimal value. Next, using the best fit value of  $m_{\text{OFS}}^*$ , we calculate  $T_D$  from the gradient of the best fit straight line of  $\log_e A_p$  versus  $B_p$ , as shown in the inset of Fig. 5. Here  $A_p$  and  $B_p$  are the ordinate and abscissa co-ordinates of the local maxima in the OFS SdH data, respectively. Using this fit we find  $T_D = 35 \pm 2$  K for  $\theta = 0^\circ$ . This value of  $T_D$  corresponds to an electron scattering time  $\tau = (3.5 \pm 0.2) \times 10^{-14}$  s, in reasonable agreement to the value of  $(6.8 \pm 0.4) \times 10^{-14}$  s derived from the two carrier Hall mobility fit for the OFS.

We compare the measured  $A_k^{\text{OFS}}$  and  $m_{\text{OFS}}^*$  values with the theoretical  $\theta$ -dependencies for the OFS in Fig. 6. Good agreement is found again between the experimental data and theory, although a slight disparity is found for  $A_k^{\text{OFS}}$  at larger  $\theta$ . This can be caused by corrugations in the sample, which combined with the strong  $\theta$  dependence of the SdH amplitude, would tend to skew the value of  $F_{\text{OFS}}$  extracted from the FFT analysis towards the value of  $F_{\text{OFS}}(\theta = 0^\circ)$ . At large  $\theta$  these relatively high frequency SdH oscillations are more challenging to measure. This is a natural consequence of the intrinsic quasi-two-dimensional nature of the BiTeI crystal structure, where the large orbit OFS quantum oscillations are only observed if  $\omega_c \tau > 1$ . This can be further exacerbated by  $c$ -axis delamination, leading to highly anisotropic extrinsic scattering.

Therefore, to extend the range of angles available, higher field measurements were also carried out for sample #2. In this case the sample was measured at 100 kHz with a 5 mA excitation current using a non-destructive pulsed magnet to 57 T (pulse duration = 36 ms). As shown in Fig. 6, including high field data for sample #2 at  $\theta = 45^\circ$ , we find good agreement between the theoretical and experimental  $A_k^{\text{OFS}}(\theta)$ .

It is worth noting that our calculations indicate that for the whole range of  $\theta$ ,  $m_{\text{IFS}}^*$  is substantially smaller than  $m_{\text{OFS}}^*$ . Such a difference is more pronounced for  $\theta \leq 40^\circ$ , where  $m_{\text{OFS}}^*$  is approximately 10 times larger than  $m_{\text{IFS}}^*$ . We attribute this to the different dispersion relations between the IFS and OFS. While for the latter, the bands are quadratically dispersive (in the plane perpendicular to the  $c$ -axis), due to the strong  $k$ -linear RSOC effect near the Dirac point, the inner bands obey a nearly linear dispersion relation. As a result the IFS carriers are much lighter than the OFS ones. Also we note that due to the shapes of the two FSs, there is no significant azimuthal anisotropy in the theoretical  $A_k$  and mass as a function of  $\theta$  for the IFS, and only slight variation at large  $\theta$  for the OFS, as shown in Figs. 4 and 6 respectively, all of which are below our experimental resolution. Thus careful alignment of the crystal in the azimuthal direction is not required to map out the shape of the FS in the  $\theta$ -plane.

Combining these results for the OFS and IFS, and the agreement with the theoretical calculations for both samples, we can conclude that the FS of this BiTeI crystal is strongly perturbed by a large internal, *bulk* RSOC, providing a non-surface-sensitive measure of the whole crystal. The bulk nature of the large spin-orbit coupling effect in BiTeI has important possible applications. The availability of a robust RSOC can be utilized as a basis to combine with other forms of electronic order such as magnetism and superconductivity. One possibility is the use of BiTeI in proximity effect studies with conventional superconductors, where non-trivial superconducting order parameters may be created,[21, 22] analogous to the interactions of Cooper pairs and the strong internal magnetic fields of magnetic systems.[23] This may be achieved by bulk synthesis (for example using doping and/or intercalation), or by *ex – situ* combinations with other crystals or thin film heteroepitaxy.

This research is supported by the Japan Society for the Promotion of Science through the ‘Funding Program for World-Leading Innovative R&D on Science and Technology (FIRST Program)’, initiated by the Council for Science and Technology Policy. C.B. and H.Y.H. acknowledge support by the Department of Energy, Office of Basic Energy Sciences, Materials Sciences and Engineering Division, under contract DE-AC02-76SF00515.

---

[1] N. W. Ashcroft and N. D. Mermin, *Solid State Physics* (Holt-Saunders, 1976).

[2] E. Bauer, G. Hilscher, H. Michor, C. Paul, E. W. Scheidt, A. Griбанov, Y. Seropegin, H. Noël,

- M. Sigrist, and P. Rogl, Phys. Rev. Lett. **92**, 027003 (2004).
- [3] J. Sinova, D. Culcer, Q. Niu, N. A. Sinitsyn, T. Jungwirth, and A. H. MacDonald, Phys. Rev. Lett. **92**, 126603 (2004).
- [4] C. L. Kane and E. J. Mele, Phys. Rev. Lett. **95**, 226801 (2005).
- [5] X.-L. Qi and S.-C. Zhang, Rev. Mod. Phys. **83**, 1057 (2011).
- [6] S. Datta and B. Das, Appl. Phys. Lett. **56**, 665 (1990).
- [7] J. Nitta, T. Akazaki, H. Takayanagi, and T. Enoki, Phys. Rev. Lett. **78**, 1335 (1997).
- [8] I. Gierz, T. Suzuki, E. Frantzeskakis, S. Pons, S. Ostanin, A. Ernst, J. Henk, M. Grioni, K. Kern, and C. R. Ast, Phys. Rev. Lett. **103**, 046803 (2009).
- [9] M. Hoesch, M. Muntwiler, V. N. Petrov, M. Hengsberger, L. Patthey, M. Shi, M. Falub, T. Greber, and J. Osterwalder, Phys. Rev. B **69**, 241401 (2004).
- [10] C. R. Ast, J. Henk, A. Ernst, L. Moreschini, M. C. Falub, D. Pacilé, P. Bruno, K. Kern, and M. Grioni, Phys. Rev. Lett. **98**, 186807 (2007).
- [11] Y. A. Bychkov and E. I. Rashba, JETP Lett. **39**, 78 (1984).
- [12] K. G. Keramidas, G. P. Voutsas, A. Papazoglou, and P. I. Rentzeperis, Zeitschrift für Kristallographie **204**, 89 (1993).
- [13] A. V. Shevelkov, E. V. Dikarev, R. V. Shpanchenko, and B. A. Popovkin, J. Sol. Stat. Chem. **114**, 379 (1995).
- [14] K. Ishizaka, M. S. Bahramy, H. Murakawa, M. Sakano, T. Shimojima, T. Sonobe, K. Koizumi, S. Shin, H. Miyahara, A. Kimura, et al., Nat. Mater. **10**, 521 (2011).
- [15] D. Hsieh, Y. Xia, D. Qian, L. Wray, J. H. Dil, F. Meier, J. Osterwalder, L. Patthey, J. G. Checkelsky, N. P. Ong, et al., Nature **460**, 1101 (2009).
- [16] Y. L. Chen, J.-H. Chu, J. G. Analytis, Z. K. Liu, K. Igarashi, H.-H. Kuo, X. L. Qi, S. K. Mo, R. G. Moore, D. H. Lu, et al., Science **329**, 659 (2010).
- [17] P. D. C. King, R. C. Hatch, M. Bianchi, R. Ovsyannikov, C. Lupulescu, G. Landolt, B. Slomski, J. H. Dil, D. Guan, J. L. Mi, et al., Phys. Rev. Lett. **107**, 096802 (2011).
- [18] J. M. Ziman, *Principles of the Theory of Solids*, 2<sup>nd</sup> edition (Cambridge University Press, 1979).
- [19] M. S. Bahramy, R. Arita, and N. Nagaosa, Phys. Rev. B **84**, 041202(R) (2011).
- [20] See online supplementary information.
- [21] J. Alicea, Phys. Rev. B **81**, 125318 (2010).

[22] A. C. Potter and P. A. Lee, Phys. Rev. B **83**, 184520 (2011).

[23] M. Eschrig, Phys. Today **64**, 43 (2011).

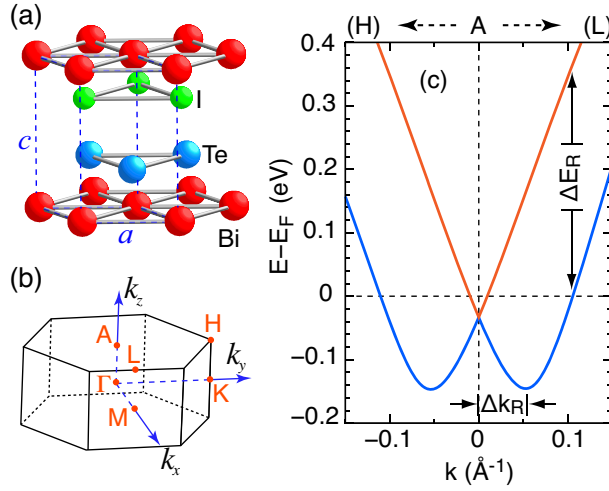


FIG. 1. (color online) (a) BiTeI crystal structure. (b) Corresponding Brillouin zone. (c) Calculated energy bands along the H-A-L direction. Local minima are offset from  $k = 0$  by  $\Delta k_R \sim 0.05 \text{ \AA}^{-1}$ , the Rashba splitting. The energy splitting  $\Delta E_R \sim 0.360 \text{ eV}$ , at the Fermi level  $E_F$ , corresponding to the density of sample #1.

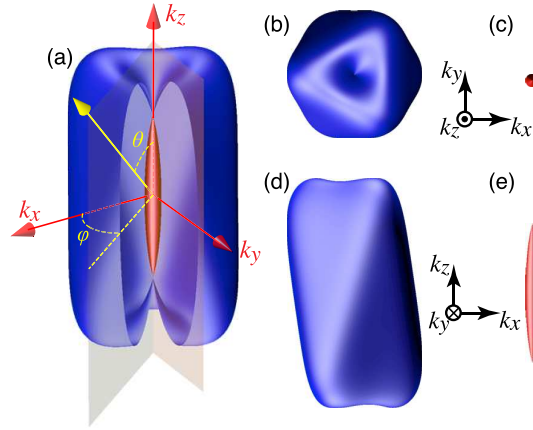


FIG. 2. (color online) Calculated Fermi surfaces around the A-point for sample #1. (a) An opened view of the outer and inner Fermi surfaces. The inclination ( $\theta$ ) and azimuthal ( $\phi$ ) angles are also shown. (b), (c) Outer and Inner Fermi surfaces, respectively, along the  $k_z$  axis, and (d), (e), along the  $k_y$  axis.

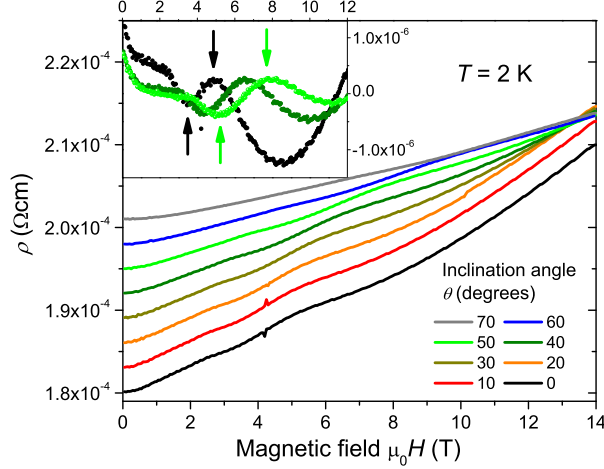


FIG. 3. (color online)  $\rho(H)$  for various values of  $\theta$  at  $T = 2$  K for sample #1. Data are offset vertically for clarity. Inset: three representative data sets with a linear background subtracted. Down (up) arrows indicate the local maximum (minimum) used to calculate the SdH oscillation frequencies for the respective data sets.

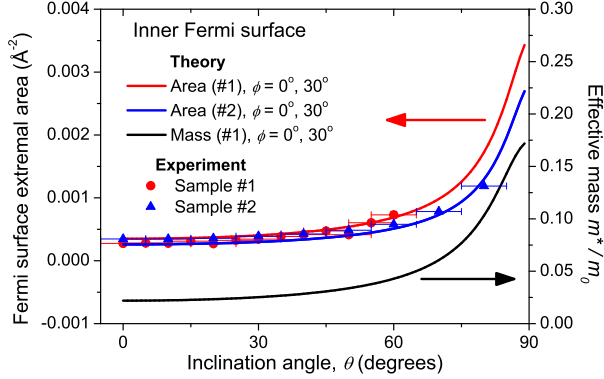


FIG. 4. (color online) Theoretical variation (solid lines) of the effective mass (right ordinate axis), and the Fermi surface area (left ordinate axis) as a function of  $\theta$ , for the IFS. Plots for theoretical azimuthal angles of  $\phi = 0^\circ$  and  $30^\circ$ , corresponding to the extremal values in the plane perpendicular to the  $c$ -axis, show no significantly different  $\theta$  dependencies. Circles (triangles) show the experimental  $A_k^{\text{IFS}}$  values extracted for sample #1 (#2). Ordinate error bars are smaller than the point size.

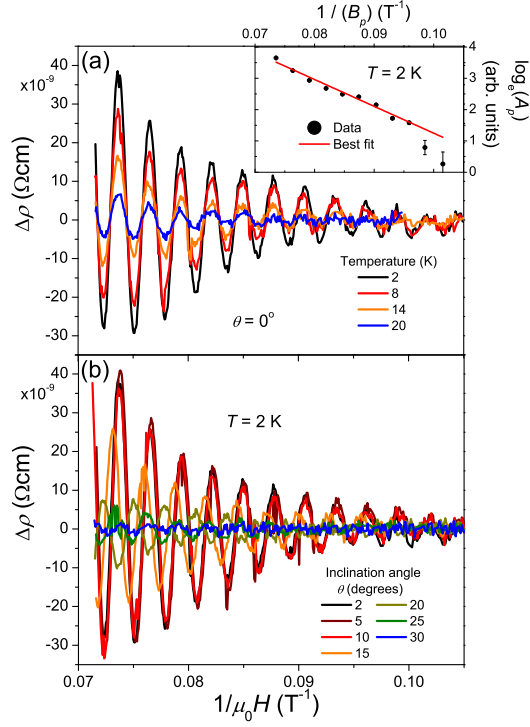


FIG. 5. (color online) Sample #1. (a) Higher frequency OFS SdH oscillations at various temperatures at  $\theta = 0^\circ$ . (b) SdH oscillations at various inclination angles for  $T = 2\text{ K}$ .  $\Delta\rho$  is the resistivity change after quartic background subtraction. Inset in (a):  $T = 2\text{ K}$ ,  $\theta = 0^\circ$ ,  $\ln(A_p)$  versus  $1/B_p$  data. Solid line is a best fit, used to determine  $T_D$ .

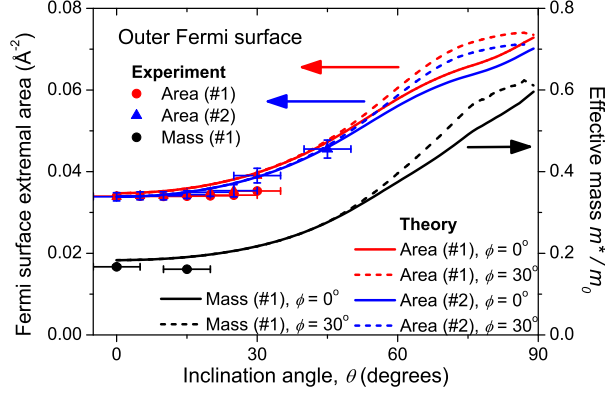


FIG. 6. (color online) Theoretical variation (solid and dashed lines) of the effective mass (right ordinate axis), and the Fermi surface area (left ordinate axis) as a function of  $\theta$ , for the OFS. Theoretical azimuthal angles are  $\phi = 0^\circ$  and  $30^\circ$ , corresponding to the extremal values in the plane perpendicular to the  $c$ -axis. Circles (triangles) show the experimental values extracted from the angular-, and temperature-dependent SdH data for sample #1 (#2). Ordinate error bars are smaller than the point size. Datum point for sample #2 at  $\theta = 45^\circ$  is calculated from SdH data up to 57 T.